AGU PUBLICATIONS

JGR

Journal of Geophysical Research: Space Physics

RESEARCH ARTICLE
10.1002/2014JA020609

Key Points:
- Significant effects of SEP effects on hydroxyl and ozone are shown
- Aura/MLS and TIMED/SABER measurements are analyzed
- Effects of concomitant geomagnetic storms are discussed

Correspondence to:
O. P. Verkhoglyadova,
Olga.Verkhoglyadova@jpl.nasa.gov

Citation:
Verkhoglyadova, O. P., S. Wang, M. G. Mlynczak, L. A. Hunt, and G. P. Zank (2015), Effects of two large solar energetic particle events on middle atmosphere nighttime odd hydrogen and ozone content: Aura/MLS and TIMED/SABER measurements, *J. Geophys. Res. Space Physics*, *120*, 12–29, doi:10.1002/2014JA020609.

Received 11 SEP 2014
Accepted 10 DEC 2014
Accepted article online 16 DEC 2014
Published online 13 JAN 2015

Effects of two large solar energetic particle events on middle atmosphere nighttime odd hydrogen and ozone content: Aura/MLS and TIMED/SABER measurements

O. P. Verkhoglyadova[1,2], S. Wang[2], M. G. Mlynczak[3], L. A. Hunt[4], and G. P. Zank[1,5]

[1]Center for Space and Aeronomic Research, University of Alabama in Huntsville, Huntsville, Alabama, USA, [2]Jet Propulsion Laboratory, California Institute of Technology, Pasadena, California, USA, [3]NASA Langley Research Center, Hampton, Virginia, USA, [4]Sciences Systems and Applications, Inc., Hampton, Virginia, USA, [5]Department of Space Science, University of Alabama in Huntsville, Huntsville, Alabama, USA

Abstract It is well established that large solar energetic particle (SEP) events affect ozone in the middle atmosphere through chemical reactions involving odd hydrogen (HO_x) species. We analyze global middle atmospheric effects at local nighttime for two large SEP events during the intervals of 7–17 November 2004 and 20–30 August 2005. Properties of the SEP events and concomitant geomagnetic storms are discussed using in situ measurements. Temporal dynamics and latitudinal distribution of HO_x and ozone densities inferred from measurements by the Aura/MLS (Microwave Limb Sounder) instrument are analyzed. We show statistically significant increases of nighttime hydroxyl (OH) density in the middle atmosphere up to $5°10^6\,cm^{-3}$ in the latitude range from 70° down to 50° latitude in northern and to −40° latitude in southern hemispheres in connection with peaks in proton fluxes of >10 MeV energy range measured by GOES spacecraft. During the storm main phases, the nighttime OH density increases were observed around ±50° in southern and northern hemispheres in the altitude range of 65–80 km. There is a correspondence between averaged nighttime OH partial column density (in 0.005 to 0.1 hPa pressure range) in the polar latitudes and energetic proton (>10 MeV) fluxes. Corresponding statistically significant nighttime ozone destructions up to 45% are observed from 70° down to 60° latitude in the northern and southern hemispheres. The SEP impulsive phases correspond to onsets of ozone density depletions. Larger relative ozone destructions are observed in the northern hemisphere in November and in the southern hemisphere in August. Simultaneous measurements of ozone density by the Thermosphere-Ionosphere-Mesosphere Energetics and Dynamics/Sounding of the Atmosphere using Broadband Emission Radiometry (TIMED/SABER) instrument independently confirm the MLS results.

1. Introduction

The solar energetic particle (SEP) events studied here are associated with flares and/or CMEs (coronal mass ejections) which erupt at the Sun, propagate outward, cause geomagnetic storms in the Earth environment, and directly impinge upon the Earth's atmosphere. The energy range of SEP particles is from hundreds of keV to above hundreds of MeV. Traditionally, SEP events are divided into impulsive events (the energetic particle population originates from solar flares) and gradual events (SEPs resulting from particles acceleration at a CME-driven shock). Impulsive events are characterized, among other things, by a sharp rise in energetic particle fluxes and a fast decay (~ several hours), whereas particle fluxes in gradual events rise slower, often exhibit a plateau and decay on the order of days. However, this distinction becomes blurred since many SEP events exhibit features of both impulsive and gradual events in a variety of physical parameters and often have impulsive and gradual phases in their time-intensity SEP profiles [*Cane et al.*, 1988; *Kallenrode*, 2003; *Li and Zank*, 2005; *Zank et al.*, 2007]. The physical characteristics of a particular SEP event are determined by a number of factors, e.g., seed population, preconditioning of the heliospheric environment (concomitant or preceding flares, preceding CMEs), and obliquity of the shock front connected to an observer [*Tylka et al.*, 2005; *Zank et al.*, 2006; *Verkhoglyadova et al.*, 2010, 2013]. The latest multispacecraft observations of longitudinally distributed SEP fluxes indicate that neither shock characteristics (including the shock obliquity which changes throughout the SEP event) nor flare preconditioning alone can explain the observed properties of SEP events [*Cohen et al.*, 2013].

In this paper we provide a general overview of the interplanetary environment during two large SEP events, starting 8 November 2004 and 22 August 2005. Both of these events were associated with CMEs and flares. This is for the first time that middle atmospheric effects of distinct impulsive and gradual phases will be studied. We will discuss a connection between the energetic particle environment observed at 1 AU and interplanetary structures encountering the Earth and the timing of concomitant geomagnetic storms. The latter is important for understanding the effective latitude range for energetic particle precipitation into the atmosphere (see below).

SEP events, in particular solar proton events (SPEs), have been shown to induce ionization chemistry in Earth's middle atmosphere that leads to a temporary enhancement in chemically active odd hydrogen species. Odd hydrogen chemical family (HO_x) includes atomic hydrogen, hydroxyl radicals (OH), and hydroperoxyl radicals (HO_2). OH plays a key role in the HO_x family throughout the middle atmosphere, while HO_2 is important at lower altitudes of the middle atmosphere and H is important at higher altitudes. Increase in odd hydrogen density causes a rapid temporary destruction of ozone (O_3). SEPs also affect ozone abundance through enhancement of odd nitrogen (NO_x) density, which is more important for lower altitudes (lower mesosphere and stratosphere) [see, for instance, *Crutzen et al.*, 1975; *Rusch et al.*, 1981; *Randall et al.*, 2001; *Jackman et al.*, 2014]. The focus of this paper is on HO_x response and its impact on ozone.

A theoretical explanation for OH nighttime density increases due to proton forcing was proposed in a pioneering study by *Solomon et al.* [1981]. One of the main reaction pathways for OH formation induced by energetic particles, e.g., protons, is through ionization and the formation of O_2^+ and $O_2^+ \cdot H_2O$. The $O_2^+ \cdot H_2O$ cluster can continue to reaction with water vapor H_2O, which leads to the following reactions: $O_2^+ \cdot H_2O + H_2O \rightarrow H_3O^+ \cdot OH + O_2$ and $H_3O^+ \cdot OH + e^- \rightarrow H + OH + H_2O$. The net result of these reactions is $H_2O \rightarrow OH + H$.

First measurements of energetic particle-induced effects on OH density were made by the Solar Mesosphere Explorer [*Solomon et al.*, 1983] following by later observations [e.g., *Jackman et al.*, 2005, 2006, 2011; *Kyrölä et al.*, 2006; *Verronen et al.*, 2006, 2007; *Damiani et al.*, 2008, 2009, 2010, 2012; *Verkhoglyadova and Wang*, 2013]. Daytime signatures in the OH distribution are observed when an SEP event is particularly strong. Since the chemical lifetime of HO_x in the middle atmosphere typically ranges from seconds to minutes, the species respond rapidly to external driving. It is presumed that the intensity of SPE fluxes over high-energy ranges ($>$1 MeV) corresponds to the intensity of the atmospheric response (in relative density enhancement or depletion). Hereafter, we consider SPEs as a typical component of an SEP event, for which increases of energetic proton fluxes at the Earth's orbit can be expected.

The penetration depth of energetic particles into the Earth's atmosphere as a function of the particle energy and the corresponding ionization rates were modeled by *Turunen et al.* [2009]. They showed that energetic protons (~5–20 MeV) could cause atmospheric ionization down to ~50 km altitude and directly affect the middle atmosphere chemistry. Interestingly, the ground level events (extreme and rare SEP events with increased fluxes at $>$ 100 MeV) do not show much impact on ozone [*Jackman et al.*, 2011]. The reason could simply be that the power laws-like distribution of energetic particles means that there are far few highly energetic particles than moderately energetic.

The latitudinal extent of SEP-related middle atmospheric effects is controlled by geomagnetic activity. CME-driven magnetic storms cause the auroral oval to expand and allow energetic particles to penetrate to lower latitudes. The cutoff location is the latitude at which the count rate of MeV-range protons is half of its mean value above 70° latitude. Time variations in the cutoff value are generally well correlated with the storm activity index for all amplitudes and at short (several hours) timescales [*Leske et al.*, 2001; *Smart and Shea*, 2005]. The invariant cutoff latitude can be as low as ~57° or lower for strong storms. It is important to study how changes in the middle atmosphere composition expand in latitude range during a SEP event in relation to strength and duration of a concomitant magnetic storm. In this study we use global measurements uniquely suited to address a relation between latitudinal nighttime middle atmospheric response and a timeline of geomagnetic storm.

SEP events are complex interplanetary phenomena that include solar flare particles and CME-shock-related accelerated interplanetary and solar particles. While HO_x and O_3 responses to several major SPEs have been discussed in previous studies, many questions remain as to how the detailed HO_x-O_3 chemical system responds to different SEPs and throughout CME-caused geomagnetic storms. Discrepancies between previous model results of increased ionization rates during the large SEP event of October 2003 and

observations of the O_3 response remain unresolved [*Jackman et al.*, 2009]. We present a study of the HO_x-O_3 density changes during two large SEP events that include temporal variability and latitudinal distribution, with an analysis of the underlying interplanetary structures responsible for energetic particle flux variations at the Earth's orbit and geomagnetic storm phases. We focus on nighttime measurements when photochemistry effects are negligible and the observed variability in OH is likely dominated by SEPs.

The main goals of this study are (1) to connect temporal changes in the HO_x and O_3 densities in the middle nighttime atmosphere with the timeline of an SEP event, (2) to study the latitudinal dependence of these density changes in connection with the dynamics of the corresponding geomagnetic storm, (3) to compare O_3 density measurements from different spacecraft during an SEP event, and (4) to analyze the correspondence between impulsive and gradual phases of an SEP event with the destruction of ozone.

2. Data Analysis

2.1. Satellite Data Sets

The Geostationary Operational Environmental Satellites (GOESs) Space Environment Monitor data (http://www.ngdc.noaa.gov/stp/satellite/goes/index.html) are a convenient tool to study interplanetary dynamics at 1 AU along the Sun-Earth line. We utilize measurements from the GOES energetic particle sensor to study the overall behavior of energetic proton fluxes at the Earth orbit over a broad energy range from ~ 1 MeV to above 100 MeV. The GOES extreme ultraviolet sensors provide the X-ray intensity and are used to indicate flare activity. We utilize 5 min averaged data to construct a timeline for the SEP events.

The Aura satellite was launched in July 2004 as a part of NASA's A-train group of Earth observing satellites and has a near-polar Sun-synchronous orbit with a ~705 km altitude. Aura provides daily global coverage with ~13 orbits per day. The Microwave Limb Sounder (MLS) on board the Aura spacecraft observes thermal microwave emission from Earth's "limb" (the edge of the atmosphere) viewing forward along the spacecraft flight direction, scanning its view from near the surface to ~90 km altitude every ~25 s. It provides *global* measurements of HO_x species in the stratosphere and mesosphere (~32 to 0.0032 hPa) on a daily basis during both day and night [*Waters et al.*, 2006; *Pickett et al.*, 2006a, 2006b; *Livesey et al.*, 2006]. The unique HO_x data, together with the simultaneous measurements of O_3 and other related parameters (including H_2O and temperature), make it possible to investigate the detailed mechanism of the response of the HO_x-O_3 system to solar forcing [*Wang et al.*, 2013]. O_3 profiles are retrieved at the same latitude every orbit, and 240 limb scans per orbit provide close to 3500 profiles per day. Scientifically, useful data on O_3 abundances are in the vertical pressure range from 215 to 0.02 hPa or up to ~ 75 km in altitude [*Livesey et al.*, 2008; *Froidevaux et al.*, 2008].

In this paper we utilize measurements from the SABER (Sounding of the Atmosphere using Broadband Emission Radiometry) instrument on board the TIMED (Thermosphere-Ionosphere-Mesosphere Energetics and Dynamics) satellite, which has been in operation since 2002. The satellite project was designed to study energetics, dynamics, and transport in the mesosphere and lower thermosphere. The SABER instrument is a 10-channel radiometer covering the spectral range from 1.27 μm to 15 μm in wavelength. SABER continuously scans the Earth's limb between 400 km and the Earth's surface, recording a profile of infrared radiance in each of the 10 spectral channels during the scan. We focus on the ozone mixing ratio profiles retrieved from radiance profile measurements in the infrared line of 9.6 μm [*Rong et al.*, 2009] from 20 km to ~95 km altitude in the day and to ~100–105 km altitude at night. The time to record a single scan is ~50 s with a sampling distance along the satellite tracks of ~500 km. We use SABER data with the nominal vertical resolution of about 2 km. The O_3 density is derived from the volume mixing ratio profiles and atmospheric density profiles retrieved in the same scans. Note that the MLS field of view increases with increasing altitude, while the SABER field of view does not change. For detailed one-to-one comparison, it is recommended to degrade the SABER data to the MLS resolution by convolving the corresponding averaging kernels taking into account the larger MLS field of view. Here we use SABER measurements just to confirm independently the MLS results on SEP-induced ozone destructions in the altitude range below 100 km.

2.2. The SEP Event of November 2004 and Its Effects on Middle Atmospheric Hydroxyl and Ozone Content

First, we analyze the SEP event which occurred approximately from 7 to 13 November 2004. The GOES environment monitor data for the SEP event are presented in Figure 1. Figures 1a and 1b show the 5 min averaged X-ray flux from GOES-12 (Figure 1a) and the 5 min averaged energetic proton fluxes in seven energy

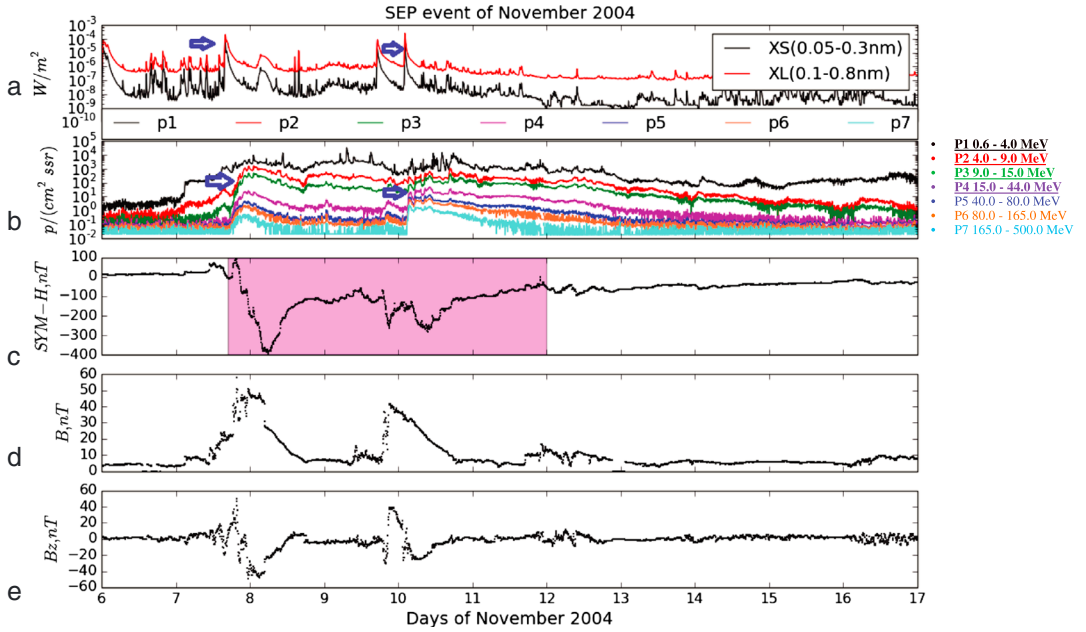

Figure 1. Interplanetary environment for the SEP event of 7–17 November 2004. (a) X-ray flux from GOES-12 averaged over 5 min intervals, (b) energetic proton fluxes in seven energy channels from 0.6 to 500 MeV measured by GOES-11, (c) *SYM-H* index, (d) interplanetary magnetic field at 1 AU in front of the Earth magnetosphere, and (e) *Z* component of the interplanetary magnetic field in GSM coordinates. Several X-class flares are shown by the blue arrows in Figure 1a and corresponding impulsive phases are shown by the blue arrows in Figure 1b. Shaded area in Figure 1c approximately indicates geomagnetic storm interval.

channels from 0.6 to 500 MeV measured by GOES-11 (Figure 1b) as a function of UT. Large SEP event onsets are observed around 8 and 10 November. X-class flares were observed at the onsets (shown by the blue arrows in Figure 1a) and could be associated with impulsive phases or sharp rises in SEP fluxes (shown by the blue arrows in Figure 1b). The SEP interval was characterized by extreme and complex geomagnetic activity reflected in the *SYM-H* index dynamics in Figure 1c. *SYM-H* is a high-resolution measure of disturbances in the symmetric ring current throughout a geomagnetic storm, which is essentially the same as the (lower resolution) *Dst* index, which indicates a level of disturbances in the Earth's magnetic field derived from measurements at several middle latitude geomagnetic observatories [*Sugiura and Hendricks*, 1967]. The approximate storm interval is shown by the shaded area. This geomagnetic activity was caused by several interplanetary structures. Figures 1d and 1e show the magnitude of the interplanetary magnetic field (IMF) at 1 AU and the geo-active B_z component of the IMF, respectively. These plots (Figures 1c–1e) are based on 5 min averaged OMNI data (http://omniweb.gsfc.nasa.gov). The largest geomagnetic storm is caused by a fast-moving CME (Figure 1d shows its magnetic field structure) with a long-lasting southward turning of the IMF B_z component to below −40 nT at the beginning of 8 November. The main phase of the storm with a minimum *SYM-H* index of −393 nT coincides with the absolute minimum of the IMF B_z (Figure 1c). Two smaller geomagnetic storms occurred at the end of 9 November and on 10 November. They are associated with another CME structure (Figure 1d) with long-duration southward IMF components (Figure 1e). Details of the interplanetary features of the November event, the geomagnetic activity, and the ionospheric storm it caused can be found in a number of papers [see, for instance, *Mannucci et al.*, 2008; *Zong et al.*, 2009; *Zuo et al.*, 2010].

The impulsive phase of the SEP events (sharp rises, especially seen in >5 MeV proton channels in Figure 1b) is followed by a gradual phase (slow decays in all energy channels), which is likely associated with particle acceleration by CME-driven shocks. Particle fluxes in lower energy channels peak later than those in higher energy channels. This is consistent with the picture of particles accelerated at a weakening shock which is decelerating as it propagates from the Sun. Sharp short-duration peaks in the lower energy proton channels (<10 MeV) could be due to the contamination of the particle detectors during large particle events. Note that the two lowest proton energy channels typically correspond to the energies of particle population trapped in the Earth radiation belt. High-energy particles arrive at 1 AU shortly after the onset of the geomagnetic storm, i.e.,

before the shock reaches 1 AU. Low-energy particle fluxes peak during the main phase of the storm when the shock arrives. This time lag between SEP peak intensities in different energy channels can help identify links between different precipitating proton populations and the middle atmosphere response. Below, we focus on MLS observations and address the question of how this complex SEP event affects middle atmospheric chemistry and ozone variability.

Figure 2 shows zonal-averaged vertical profiles of hydroxyl density as a function of time for this SEP event interval. MLS data are binned in 10° latitude bins equatorward from ±70° latitude (in both hemispheres). Nighttime data are selected using the condition solar zenith angle (SZA) $>$ 95° on the solar zenith angle (SZA) as the cutoff. Because Aura is a Sun-synchronized satellite with a polar orbit of 98° inclination, the local solar time of data acquisition during daytime/nighttime at given latitude generally has negligible changes from day/night to day/night except polar region. Simple interpolation is used to make MLS zonal mean plots. Figure 2a shows OH zonal densities averaged within a [−70°, −60°] latitude bin. Density enhancements up to 3 times the average background value occur on 8 and 9 November at approximately 70 to 80 km altitude. From Figure 1b, the first peak in SEP fluxes corresponds to the nighttime OH zonal density enhancement. The second peak in SEP fluxes around 10 November is seen mostly in $>$15 MeV frequency ranges. The impulsive SEP event is not observed in the lower energy ranges $<$15 MeV. Figure 2a does not show a corresponding OH enhancement for the second SEP event. Northern hemisphere measurements within the [60°, 70°] latitude bin show an increase in the OH density, possibly associated with the SEP event around 8–10 November (Figure 2b).

Figures 2c through 2f show nighttime zonal-averaged OH densities at lower latitudes down to ±40° in both hemispheres. There are small visible enhancements in OH density in Figures 2c–2e during the studied interval. There seems to be a certain hemispheric asymmetry of the response if we compare Figures 2a, 2c, and 2e with Figures 2b, 2d, and 2f, respectively, with a more pronounced OH density response in the southern hemisphere. However, the enhancement in the northern hemisphere is not weaker than in the southern hemisphere if we look at the duration of the enhancement and the relative change. The southern hemisphere enhancement is only seen for 1 day with larger uncertainties represented by the data precision (not shown here), while the northern hemisphere enhancement is more statistically convincing and present over consecutive days. This is consistent with simultaneous ozone destructions (Figure 4b, discussed below). Signatures in the hydroxyl abundance, which can be associated with SEPs, are seen at high to ~ 50° in NH (Figure 2d) and 40° in SH (Figure 2e). This is consistent with the minimum expected cutoff latitude for a geomagnetic storm. The enhancement seems to be a day later than the strong enhancement seen at 70–60 latitudes at 70–80 km altitudes.

Figures 3a and 3b show examples of daily nighttime zonal-averaged profiles of OH density in the [60°, 70°] and [−70°, −60°] latitude ranges. There are clear enhancements in the nighttime polar hemispheric density on 8 November compared with the preevent days, which is in agreement with OH increases (Figures 2a and 2b). The dashed lines indicate uncertainty bounds and confirm that the peak values are statistically significant for these days. The nighttime-averaged zonal profiles of OH density in the [60°, 70°] latitude range peak on 8–10 November (see Figures 3a and 2b). Enhancements in individual nighttime density profiles up to $5°10^6$ cm^{-3} are also seen within the [−60°, −50°] and [−50°, −40°] latitude bins (not shown to save space). The "spiky" vertical profiles in Figure 3b as compared to Figure 3a are likely an averaging artifact. There are fewer data points corresponding the nighttime criteria SZA $>$ 95° in the southern hemisphere than in the northern hemisphere for the November 2004 event. Results for other latitude bins do not show statistically significant enhancements in the vertical density profiles.

Figure 4 presents the corresponding variability from the preevent mean of the zonal-averaged profiles for ozone (O_3). The variability is calculated using the 3 day mean before the onset of the event as the background value. Positive values mean a reduction in O_3. Figure 4a shows nighttime (SZA $>$ 95°) ozone destructions in the [−70°, −60°] latitude bin during the SEP interval. The uncertainty of the variability from the mean (calculated through the error propagation of the measurement precisions) is large (~35%) (shown in Figure 4e) at high altitudes near South Pole during this time of year (due to the short nighttime and fewer nighttime profiles). We cannot draw a quantitative conclusion for this ozone destruction. Nevertheless, the comparison of Figure 4a with its error bar in Figure 4e suggests an ozone destruction qualitatively. Nighttime ozone density variability in the [60°, 70°] bin shows a pronounced enhancement of ~45% during the SEP event interval (Figure 4b). Examination of daily zonal-averaged profiles with the measurement uncertainties (below 10%, Figure 4f) shows that the result is statistically significant. This result is consistent with the OH

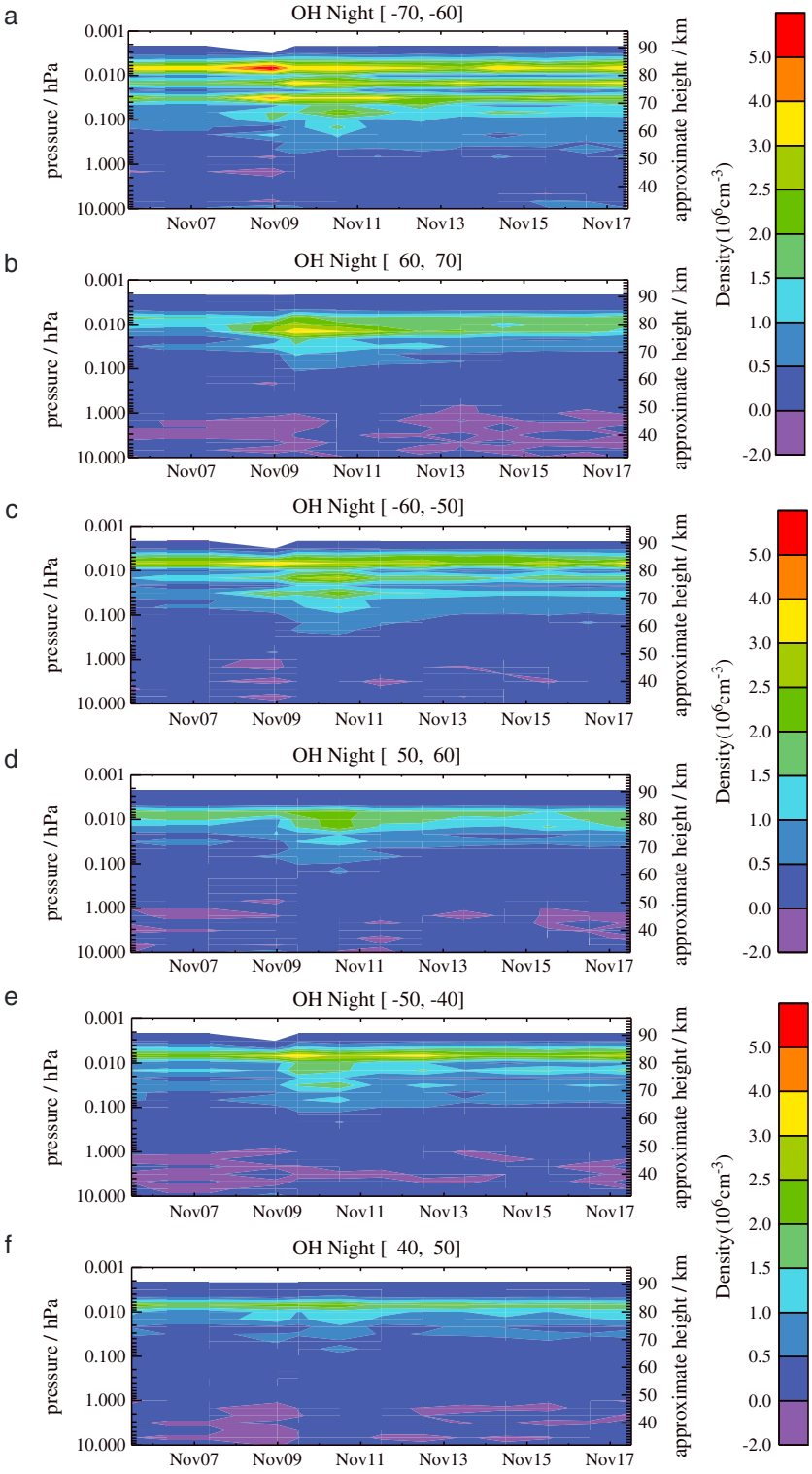

Figure 2. Aura/MLS zonal-averaged vertical profiles of hydroxyl density for the November 2004 SEP event interval during local nighttime (SZA > 95°). Data are binned in several latitude bins: (a) [−70°, −60°], (b) [60°, 70°], (c) [−60°, −50°], (d) [50°, 60°], (e) [−50°, −40°], and (f) [40°, 50°].

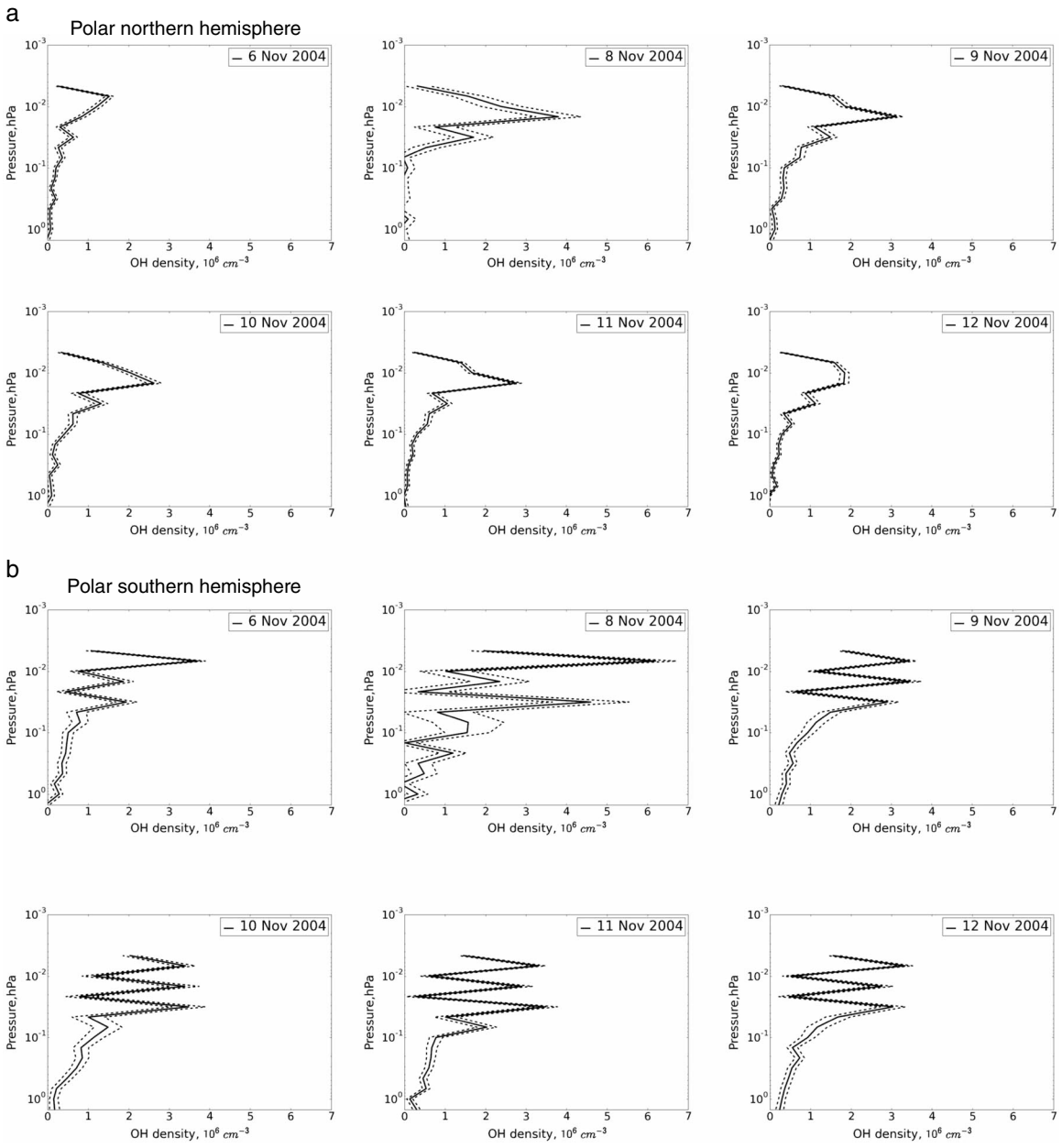

Figure 3. Nighttime zonal profiles of OH density for the November 2004 SEP event averaged over a day and latitude bins (a) [60°, 70°] and (b) [−70°, −60°]. Dashed lines show error bounds.

density increase shown in Figure 2b. Figures 4c and 4d show nighttime ozone variability in the [−60°, −50°] and [50°, 60°] latitude bins, respectively. The ozone density shows very little variability in the [−50°, −40°], [40°, 50°] (not shown here), and [−60°, −50°] latitude bins. Ozone destruction is larger in northern hemisphere.

To further confirm the ozone destruction observed by MLS, we also investigated the SEP event using SABER measurements. Figure 5 shows examples of daily SABER coverage (location of tangent points in latitude and longitude) on 10 November 2004 (blue dots) and 23 August 2005 (red triangles; see below). For the November 2004 event, SABER had good coverage of the high-latitude northern hemisphere and did not go beyond −60° in the southern hemisphere. All nighttime measurements (with SZA > 95°) of ozone density profiles are averaged in longitude and binned in the same latitude bins as those for the MLS data analysis.

Figure 6 show the zonal-averaged nighttime O_3 density profiles in the [60°, 70°] (Figure 6a), [50°, 60°] (Figure 6b), and [−60°, −50°] (Figure 6c) latitude bins for 10 days in November 2004. We focus on the altitude

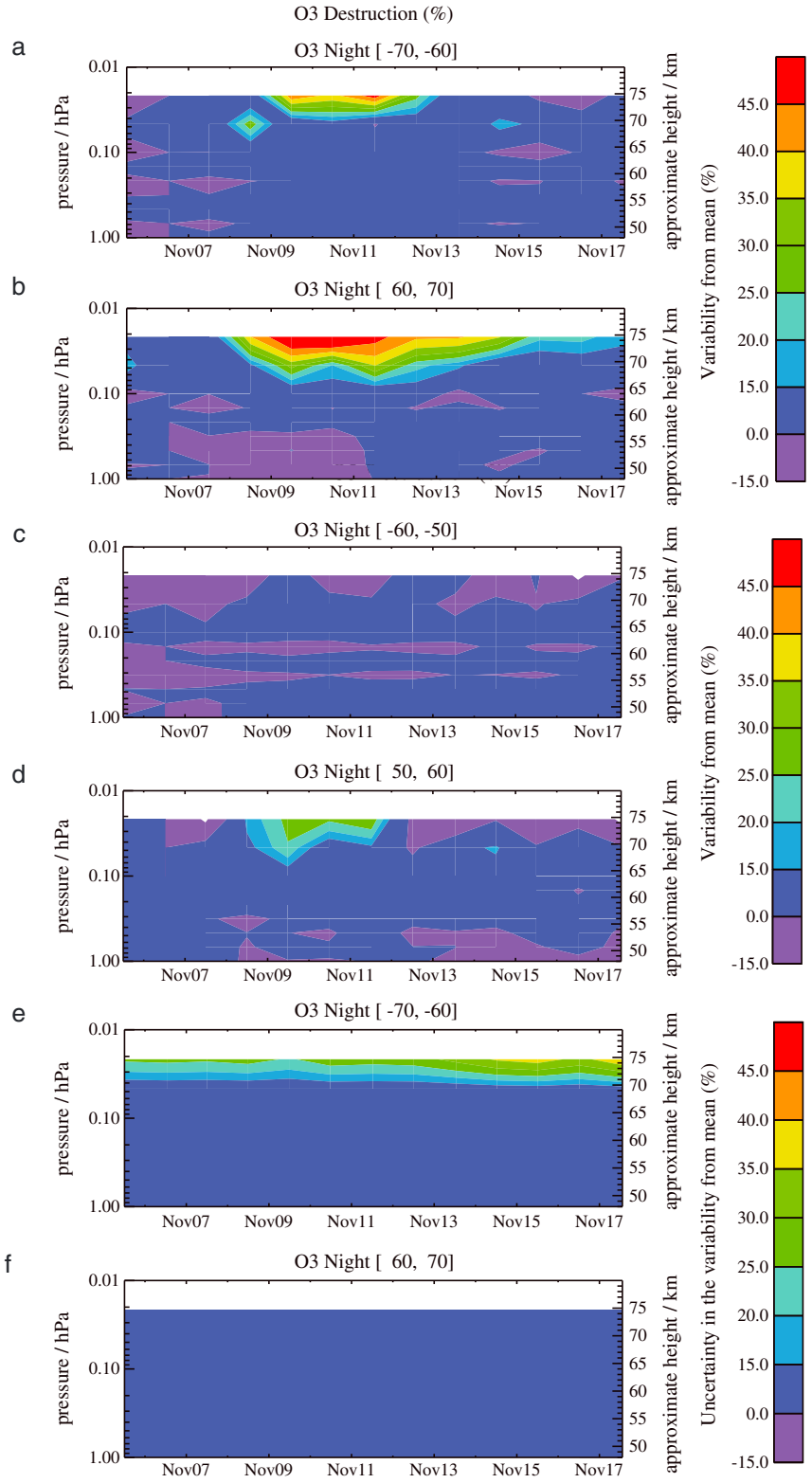

Figure 4. Variability from the mean of zonal-averaged profiles of ozone (O_3) for the November 2004 SEP event at local nighttime (SZA > 95°). Data are averaged over the latitude bins (a) [−70°, −60°], (b) [60°, 70°], (c) [−60°, −50°], and (d) [50°, 60°]. Positive values mean reduction in O_3. (e, f) Uncertainties in the calculated variability from the mean for the latitude bins [−70°, −60°] and [60°, 70°]. See the text for details.

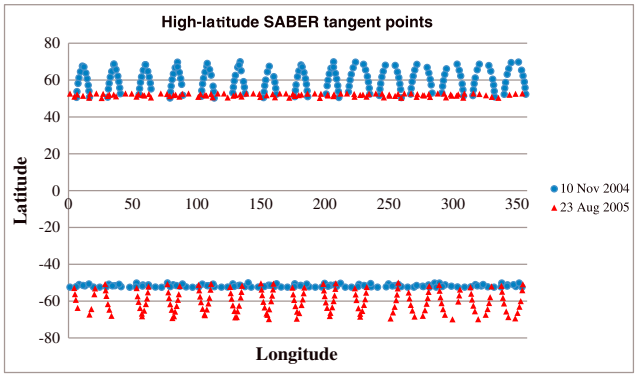

Figure 5. Daily SABER coverage (location of tangent points in latitude and longitude) on 10 November 2004 (blue dots) and 23 August 2005 (red triangles).

range from 65 km to 75 km (indicated by the boxes on the panels) where the MLS measurements showed SEP effects on the O_3 content. According to *Damiani et al.* [2010], this altitude range shows the highest correlation between SEP fluxes and hydroxyl density increases. Zonal-averaged profiles for the [60°, 70°] bin show that the maximum density in this altitude range was measured on 7 November before the SEP event (Figure 6a, black squares). Large decreases in the O_3 density occurred on 8–11 November during the peak SEP event. A sudden O_3 density depletion occurred on 8 November (red circles) followed by the largest density depletion of the event which occurred on 9 November (blue triangles). The ozone destruction coincides with a peak in SEP flux (Figure 1b). The density starts to recover on 10–11 November with values being close to those of 8 November and approaches the preevent background on 17 November. The profile dynamics presented here agrees with the dynamics of the averaged zonal OH profiles derived from MLS measurements (compare with Figure 3a). Note large error bars for MLS-derived profile on 8 November (Figure 3a), while actual OH peak values on 8 and 9 November could be about the same. The maximum relative O_3 destruction derived from SABER measurements from 7 to 9 November is ~35% at 73 km altitude. This result is consistent with the ozone density depletions and OH density increases observed by MLS (see Figures 4b and 2b). A validation study for ozone measurements on TIMED/SABER by *Rong et al.* [2009] concluded that nighttime measurements have a precision of ~ 5% above 65 km altitude in high-latitude regions.

Similar dynamics for O_3 is observed for the [50°, 60°] latitude bin (Figure 6b), but the ozone density depletions are much weaker and consistent with small OH density increases in MLS data (Figure 2d). Note an increase in density values at ~80 km from 7 November. O_3 density depletions in the [−60°, −50°] latitude bin (Figure 6c) are much smaller than in the northern hemisphere (consistent with MLS measurements in Figures 4c and 4d).

2.3. The SEP Event of August 2005 and Its Effects on Middle Atmospheric Hydroxyl and Ozone Content

The SEP event of August 2005 is characterized by three prominent X-class flares on 22 and 23 August 2005 seen in Figure 7a. The event had several peaks in energetic proton flux (Figure 7b). The onsets of the first two, on 22 and 23 August, coincide with two large X-class flares. SEP fluxes in the energy ranges greater than 4 MeV peak on 23 August (shown by the blue arrow, Figure 7b). The most elevated lower energy (<4 MeV, black curve) SEP fluxes were observed on 24 August. The concomitant isolated geomagnetic storm had a minimum *SYM-H* value of ~ −174 nT on 24 August (shown in Figure 7c). The shaded area of Figure 7c approximately indicates the geomagnetic storm interval. The storm was caused by a CME (the IMF structure is seen in Figure 7d) with a large southward excursion of the IMF B_z component (Figure 7e). A detailed analysis of interplanetary parameters and their space weather consequences for this storm interval can be found, for instance, in *Sreeja et al.* [2009]. The peak in the low-energy SEP event is coincident with the CME shock arrival at the Earth. The SEP event of August 2005 is somewhat less intense than the SEP event discussed above.

Figure 8a shows that the nighttime OH density increase in the [−70°, −60°] latitude bin during the SEP interval of 23–25 August is weak. However, the missing data and the corresponding gaps in the time series in Figure 8a due to temporary instrument anomalies result in interpolated plot that may not reflect peak density changes. There is a pronounced nighttime density increase within the [60°, 70°] bin that occurred in the altitude range of 70–80 km (Figure 8b). Analysis of the vertical profiles gives peak values of up to $5°10^6$ cm^{-3} beyond the error bars. The nighttime OH density increases in the rest of the latitude bins (40° to 60° and −60° to −40°) were very weak and some of the northern hemisphere high-latitude data were noisy (Figures 8c–8f).

The zonal-averaged O_3 density for this SEP event is shown in Figure 9. There are strong nighttime density depletions of up to 40% in the [−70°, −60°] latitude bin on 24–25 August, and this result is statistically

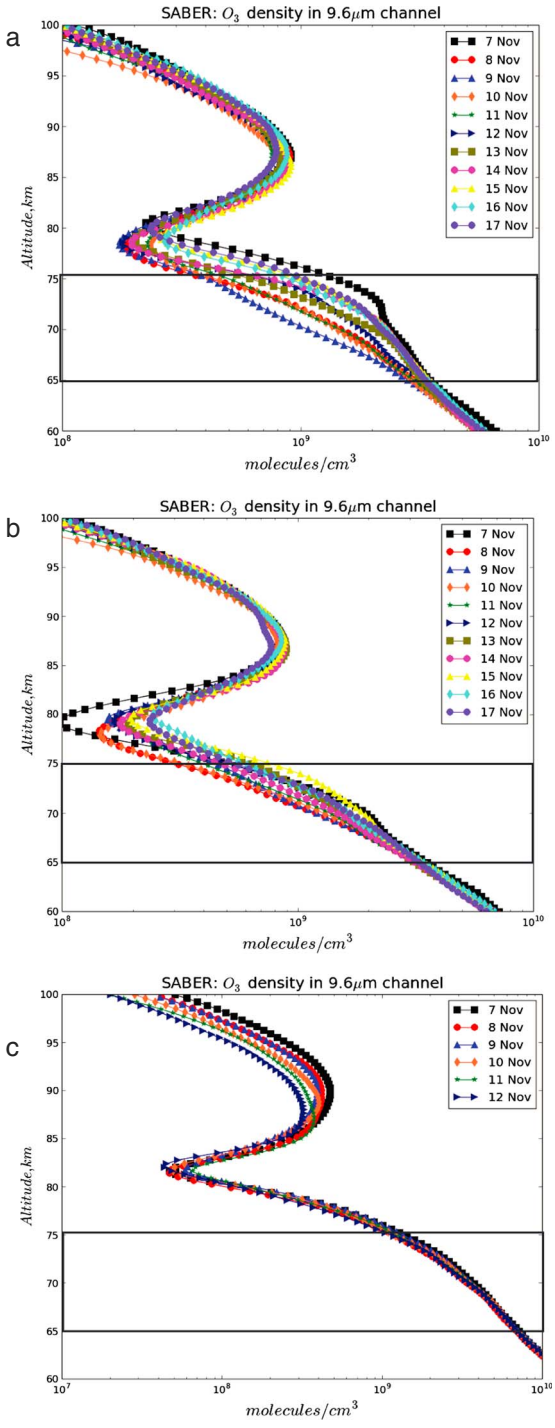

Figure 6. Daily averaged zonal nighttime (SZA > 95°) O_3 density profiles in (a) [60°, 70°], (b) [50°, 60°], and (c) [−60°, −50°] latitude bins for 7−17 November 2004. The altitude range from 65 km up to 75 km is indicated by the boxes on the panels.

significant with an uncertainty of less than 10% (Figures 9a and 9e). Weaker depletions in the northern high latitudes [60°, 70°] (with short nighttime and thus fewer nighttime data at this time of year) are observed with a greater uncertainty of ~25% (Figures 9b and 9f) and may not be statistically significant. There are no pronounced nighttime O_3 density depletions within the [−60°, −50°] and [50°, 60°] latitudes during the SEP event (Figures 9c and 9d). The event exhibits a hemispheric asymmetry with more pronounced O_3 density effects in the southern hemisphere.

The zonal-averaged daily nighttime SABER ozone profiles for 20–29 August 2005 are shown in Figure 10. The SABER orbit did not allow sampling of the northern high latitudes but provided good coverage in the southern high latitudes (Figure 5, red triangles). Figure 10a shows data from the [−70°, −60°] latitude bin. The altitude range of 65–75 km is indicated by the boxes in the panels. The preevent background density is observed on 20–22 August. The largest O_3 density depletions (up to ~40%) at the MLS altitude range of 65 to 75 km are observed on 23–24 August. The three profiles for these dates are almost identical and occurred during the peak SEP flux interval (see Figure 7b). The density profiles recover to almost preevent values by 25 August. Similar dynamics are observed in the [−60°, −50°] latitude bin (Figure 10b), but the effects are weaker than at higher latitudes. Note complex dynamics of the density around ~80 km altitude in this latitude range. The largest destruction in this altitude range occurs on 23 August, but the difference between profiles is small. There is a very small difference in the vertical profiles at [50°, 60°] latitudes with about a 15% density change (Figure 10c), in agreement with the weak effect observed in the MLS O_3 data (Figure 9d).

3. Discussion

Analyses of zonal-averaged OH and O_3 density profiles from MLS measurements show a statistically significant connection with the timeline and fluxes of SEP events, OH density increases, and ozone destructions. For the November 2004 SEP event, we observed nighttime destructions of above 45% O_3 in the northern high latitudes throughout 9 to 12 November (Figure 4b). A weaker effect was observed in the southern latitudes (Figure 4a). The destructions occur mostly in the 65–75 km altitude range. Note that MLS ozone data can be used up to ~75 km altitude [*Livesey et al.*, 2008]. For the August 2005 event, nighttime O_3 destructions

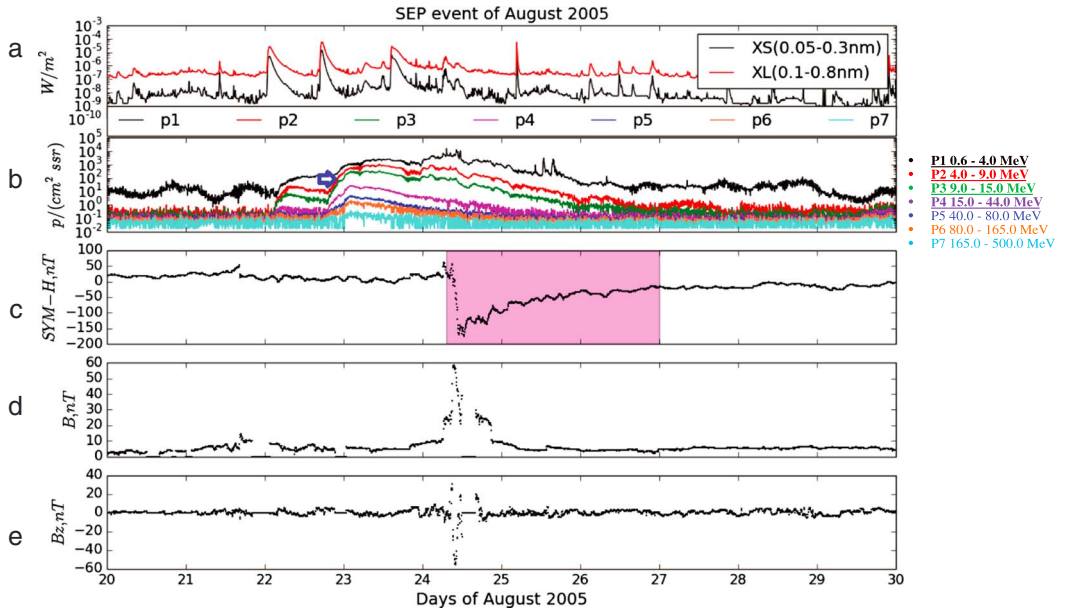

Figure 7. Interplanetary environment for the SEP event of 20–30 August 2005. (a) X-ray flux from GOES-12 averaged over 5 min intervals, (b) energetic proton fluxes in seven energy channels from 0.6 to 500 MeV measured by GOES-11, (c) *SYM-H* index, (d) interplanetary magnetic field at 1 AU in front of the Earth magnetosphere, and (e) *Z* component of the interplanetary magnetic field in GSM coordinates. The largest impulsive phase of SEP event is shown by the blue arrow in Figure 7b. Shaded area in Figure 7c approximately indicates geomagnetic storm interval.

reached 40% in the southern high latitudes on 23–24 August (Figure 9a). Atmospheric effects were weaker in the northern hemisphere (Figure 9b).

There is a hemispheric asymmetry in that larger ozone destructions are observed in the northern hemisphere after the autumn equinox into winter and in southern hemisphere after the spring equinox into summer. Since there is no clear asymmetry in OH measurements (within the measurement error), we suggest that it is primarily to ozone only. We suggest that observed hemispheric asymmetry in percentage ozone destruction is mainly due to the different background nighttime ozone levels in the two hemispheres as a result of the seasonal variations of ozone. Statistical analysis of nighttime SABER O_3 observations in January and July over several years of observations revealed that the maximum mesospheric ozone occurrence area shifted toward the northern hemisphere in July and toward the southern hemisphere in January [*Rong et al.*, 2009]. For example, the November event corresponds to early winter in northern hemisphere and early summer in southern hemisphere, respectively. The nighttime ozone level at this time of year is significantly higher in the southern hemisphere than in the northern hemisphere. The relative ozone destruction as a result of SPE-induced HO_x enhancement is thus more pronounced in the northern hemisphere where background ozone level is lower. Thus, the same ozone abundance change in the northern hemisphere in winter will be seen as relatively larger compared to the southern hemisphere for this event.

Our results suggest that the impulsive phase of SEP events (seen in proton channels $>$10 MeV) cases sudden ozone destructions. For the August 2005 event we observed a destruction that lasted about 3 days in the high-latitude southern hemisphere (Figure 10a). The timing agrees with the gradual phase of the SEP event (Figure 7b). Ozone destructions for the November 2004 event in the high northern latitudes (Figure 4b) correspond to the gradual phase of the SEP event (Figure 1b). Thus, the impulsive phase of an SEP event could indicate the onset of the ozone event seen in the 65–75 km altitude range, which is sustained through the gradual phase of an SEP event as long as the 10 MeV and greater proton energy range stays elevated.

To address the dynamics of the hydroxyl response throughout an SEP event, we plot GOES proton fluxes in the energy range above 10 MeV together with nighttime zonal OH partial column density in the pressure range of 0.005 to 0.1 hPa (approximately ~65–85 km altitude range) in Figure 11. Results for the latitude bins [60°, 70°] and [−70°, −60°] for the November 2004 event are shown in Figures 11a and 11b, correspondingly. There is a

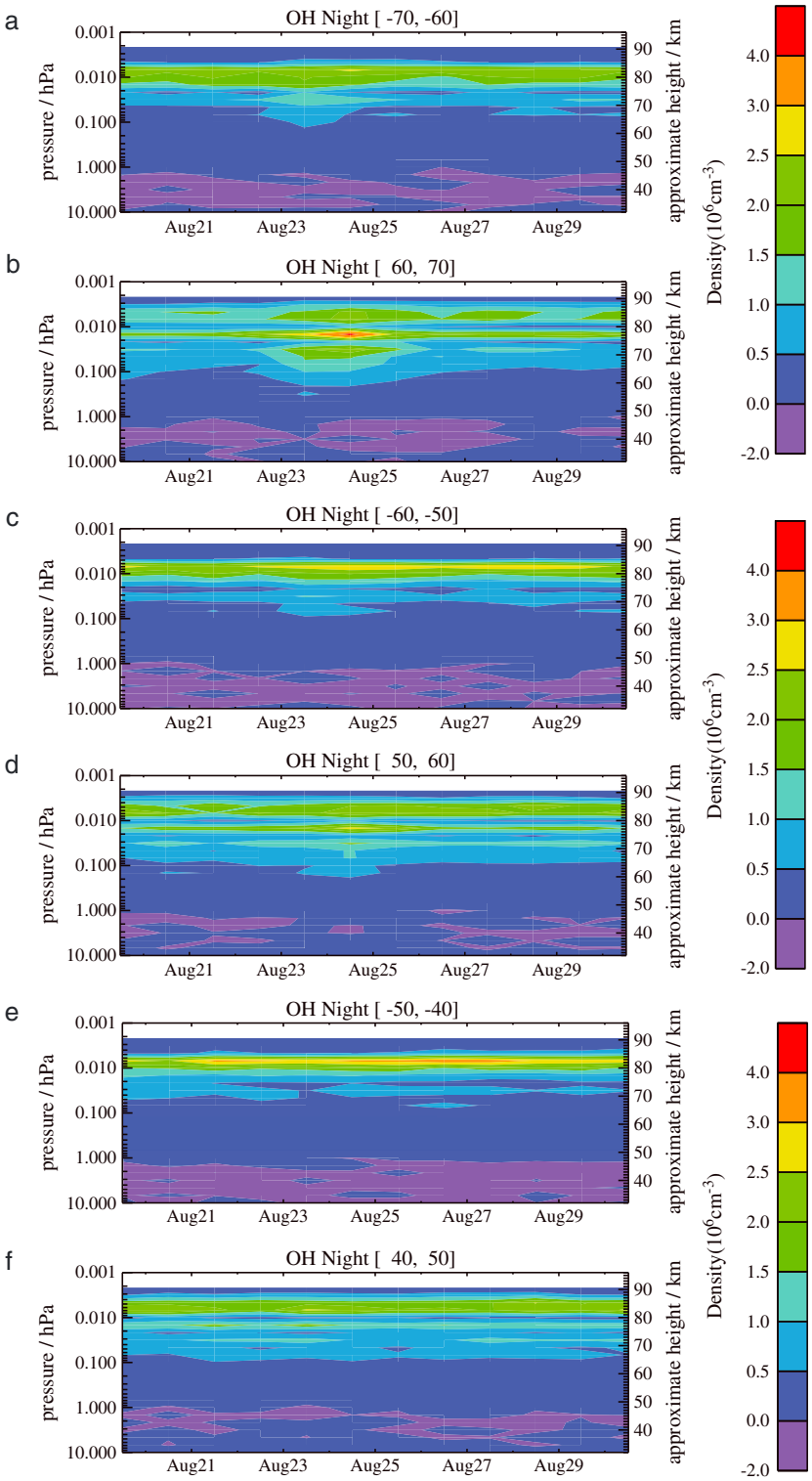

Figure 8. Aura/MLS zonal-averaged vertical profiles of hydroxyl density for the August 2005 SEP event interval during local nighttime (SZA > 95°). Data are binned in several latitude bins: (a) [−70°, −60°], (b) [60°, 70°], (c) [−60°, −50°], (d) [50°, 60°], (e) [−50°, −40°], and (f) [40°, 50°].

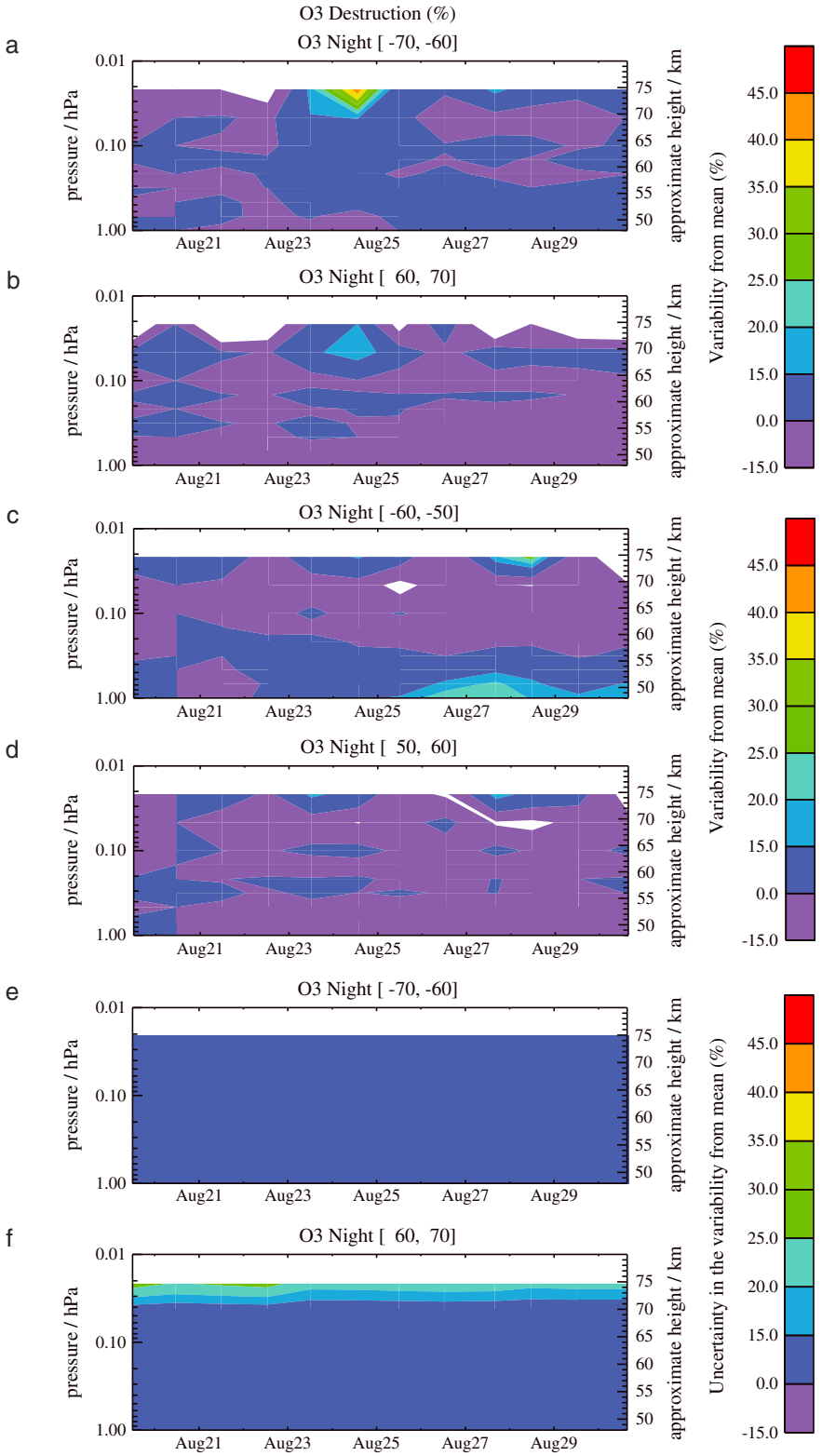

Figure 9. Variability from the mean of zonal-averaged profiles of ozone (O_3) for the August 2005 SEP event at local nighttime (SZA > 95°). Data are averaged over the latitude bins (a) [−70°, −60°], (b) [60°, 70°], (c) [−60°, −50°], and (d) [50°, 60°]. Positive values mean reduction in O_3. (e, f) Uncertainties in the calculated variability from the mean for the latitude bins [−70°, −60°] and [60°, 70°]. See the text for details.

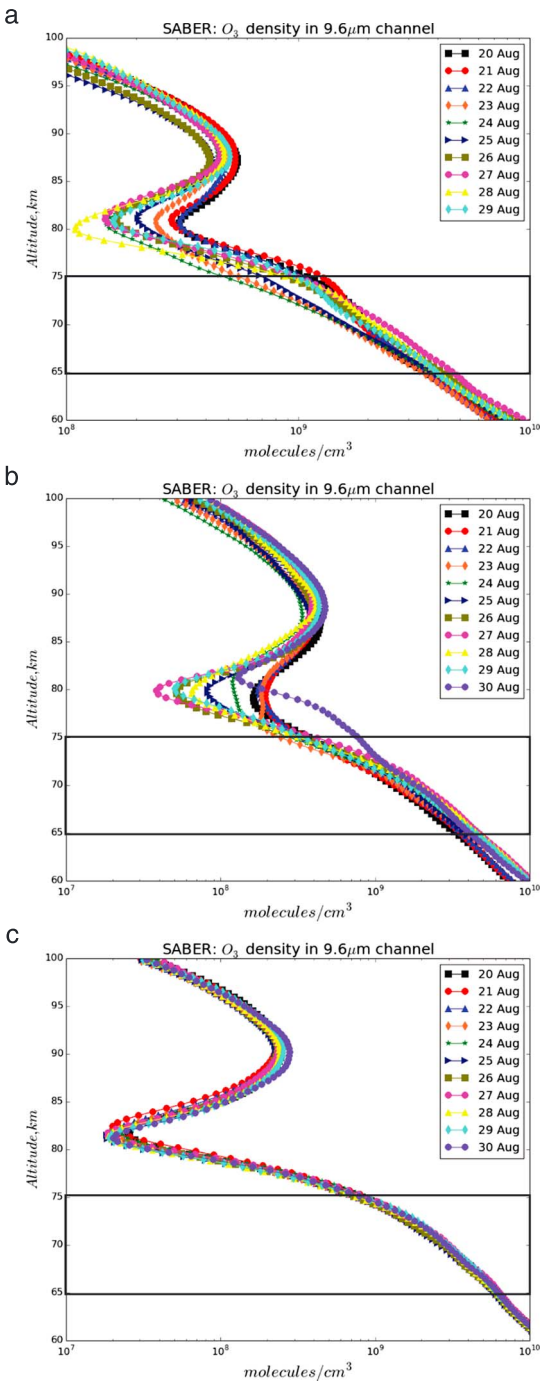

Figure 10. Daily averaged zonal nighttime (SZA $>$ 95°) O_3 density profiles in (a) [−70°, −60°], (b) [−60°, −50°], and (c) [50°, 60°] latitude bins for 20–29 August 2005. The altitude range from 65 km up to 75 km is indicated by the boxes on the panels.

distinct correlation between enhanced OH nighttime density (error bars not shown) and energetic proton fluxes during the SEP event. This result is consistent with the correlation study by *Damiani et al.* [2010]. The OH density response is more pronounced in the polar northern hemisphere (up to 100% relative change from the preevent background) than in the southern hemisphere (~ 40% relative change from the preevent background) for this SEP event. Comparison between GOES fluxes and nighttime zonal OH partial column density for the August 2005 event are shown in Figures 11c and 11d for the northern high latitudes and the southern high latitudes, correspondingly. There is a distinct response in OH column density to SEP flux. Again, average response is stronger in the northern hemisphere (~80% of the background value) as compared to the southern hemisphere (~40% of the background value).

OH column density remains elevated for several days after the SEP event of November 2004 (Figures 11a and 11b). The chemical lifetime of odd hydrogen in the middle atmosphere is up to minutes. One possible mechanism for the nighttime OH density enhancement after the SEP event could be due to the precipitation of loss-cone electrons (with energies $>$100 keV to affect mesosphere at 80 km), subsequent atmosphere ionization, and water cluster ion chemistry. *Verronen et al.* [2011] provided the first evidence of mesospheric OH response to electron precipitation from the radiation belts, followed detailed studies and comparison between model and observational signals for both OH and ozone [*Verronen et al.*, 2013]. Typically, the peak ionization rates due to energetic electron precipitation are about an order of magnitude lower than for the largest SPE. *Andersson et al.* [2012] thoroughly investigated all OH enhancements connected to radiation belt electrons during the MLS measurement period 2009–2014 and further studied the latitudinal dependence of the effects [*Andersson et al.*, 2014].

We do not observe clear effect of elevated postevent OH densities for the SEP event of August 2005 (Figures 11c and 11d) within the measurement uncertainty. If energetic precipitating electrons are the cause, this could be explained by relative strength and duration (double storm) of the geomagnetic storm of November 2004 as compared to the geomagnetic storm of August 2005 (see Figures 1 and 7).

Odd hydrogen nighttime density that increases up to $5°10^6\,cm^{-3}$ were observed in the latitude range from 70° down to 40° latitude in SH but only down to 50° latitude in NH (Figures 2). The timing of the density

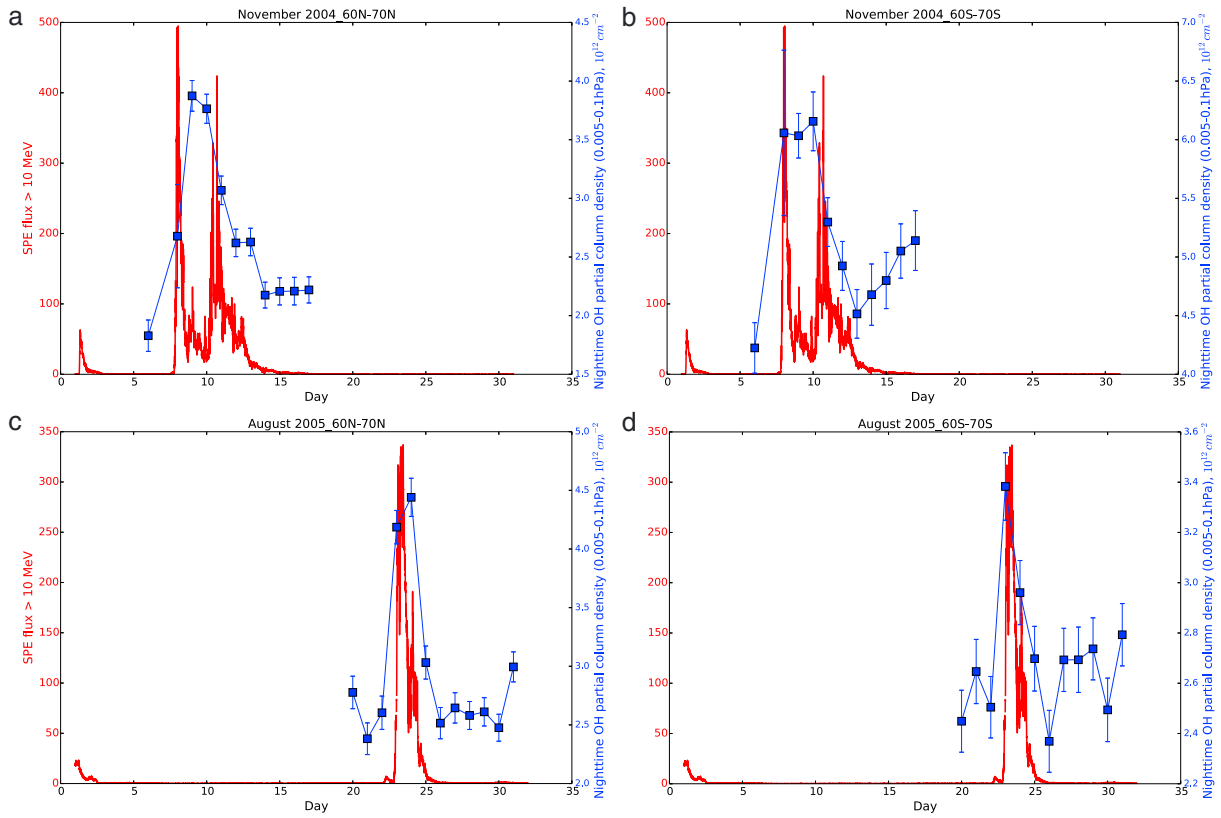

Figure 11. Energetic proton flux (>10 MeV) measured on GOES-11 and nighttime zonal OH partial column density in the pressure range of 0.005 to 0.1: (a) November 2004 event in the latitude bin [60°, 70°], (b) November 2004 event in the latitude bin [−70°, −60°], (c) August 2005 event in the latitude bin [60°,70°], and (d) August 2005 event in the latitude bin [−70°, −60°].

enhancements corresponds with ozone destructions and the timeline of SEP events. Careful examination of Figures 1b, 2b, and 3a for the high-latitude northern hemisphere shows that the OH density increase occurring around 80 km on 9 November corresponds in timing to peak values of the proton flux in the lowest energy range (up to 4 MeV, black curve). The two smaller density increases that occur around 70 to 75 km on 8 and 10 November which approximately coincide in time with peaks of the SEP flux at a higher energy range (above 15 MeV, green curve). According to modeling by *Turunen et al.* [2009, Figure 3] energetic protons with energies up to 4 MeV can penetrate down to ~75 km in altitude. More high-energy particles (>10 MeV) can precipitate below 70 km. This is consistent with observations of hydroxyl at high latitudes [*Damiani et al.*, 2010].

The latitudinal extent of the middle atmospheric response is determined by the cutoff latitude for a specific geomagnetic storm concomitant with the CME-induced gradual phase of an SEP event. According to observations by *Leske et al.* [2001], geomagnetic storms with *SYM-H* ~ −150 nT could reduce the cutoff latitude to 57°. Study of nighttime zonal-averaged profiles of hydroxyl show SEP-related signatures down to bins of [−50°, −40°] and [50°, 60°] in latitude in the southern and northern hemispheres for the 8 November 2004 event (Figures 2e and 2d) and down to [−60°, −50°] and [50°, 60°] for the 24 August 2005 event (Figures 8c and 8d). The main phases of the geomagnetic storms indicated by the *SYM-H* minima (see Figures 1c and 7c, within the shaded areas) occurred on these days. The August storm was weaker than the November storm (compare minimum *SYM-H* index values in Figures 1c and 7c). A detailed modeling study of the longitudinal extent of atmospheric signatures by *Verronen et al.* [2007] indicated a lower boundary for the cutoff latitude as 57°. However, it is difficult to reliably estimate this parameter for the extreme storms studied here (*SYM-H* ~ −400 nT and −170 nT) due to significant deformation of the Earth's magnetosphere. It is feasible that the cutoff latitude could reach 50° and lower for very strong storms. We observed weak but statistically significant hydroxyl signatures around [−50°, −40°] for the strong storm of November 2004.

4. Conclusions

We analyzed the effects on the middle atmosphere (65 to 80 km altitude) of the SEP events of 8 November 2004 and 22 August 2005 using MLS measurements. There are pronounced increases in the nighttime hydroxyl density associated with the SEP flux event history. The altitude range where atmospheric effects are observed (70–80 km) is consistent with precipitating particles in the energy range >10 MeV. Ozone measurements show statistically significant ~45% density destructions, especially at high latitudes. We observe hemispheric asymmetry in ozone destruction with stronger relative effects in northern hemisphere for November 2004 and in southern hemisphere for August 2005 events.

Most of the previous studies [*Jackman et al.*, 2005, 2014; *Verronen et al.*, 2006; *Damiani et al.*, 2009, 2010] analyze SEP effects in the polar atmosphere. We utilized global MLS and SABER measurements to study the latitudinal extent of the middle atmosphere response to SEPs. OH density enhancements were observed by MLS down to latitudes of ±50° (or even −40° in one of the events) during concomitant geomagnetic storms, with effect at the lowest latitudes occurring during the main storm phases on 8 November 2004 and 24 August 2005. This is consistent with the minimum expected cutoff latitude for a strong geomagnetic storm [*Leske et al.*, 2001; *Verronen et al.*, 2007]. Can we expect a lower latitude extent for a superstorm? This is a subject for further modeling studies that include a restructuring of the magnetosphere during an extreme geomagnetic storm.

We analyzed O_3 measurements by SABER during these two SEP events. The largest ozone density depletions in the altitude range 65–80 km coincided with the peaks of the SEP events of 9 November 2004 and 23–25 August 2005. The maximum relative O_3 destruction derived from SABER measurements from 7 to 9 November is ~35% at 73 km altitude which is consistent with the ozone density depletions and OH density increases observed by MLS. Weaker ozone destructions were observed down to latitudes of ±50°.

We find that the middle atmosphere responds to both the impulsive and gradual phases of SEP events. The impulsive phase appears to induce a sharp enhancement of the hydroxyl density and ozone destruction in the 65–75 km altitude range, which is sustained through the gradual phase of the SEP event as long as the proton flux at and greater than the ~10 MeV energy range stays elevated. Using SABER measurements in addition to MLS measurements allows one to extend the analysis of O_3 content above ~ 75 km altitude. SABER measurements show complex variabilities of ozone density around ~80 km at high latitudes throughout the SEP events. Understanding ozone response to SEPs in this altitude region requires further study.

We showed the correspondence between the averaged nighttime OH column density in the polar latitudes and 0.005 hPa to 0.1 hPa pressure range and energetic proton (>10 MeV) fluxes during two SEP events. Figure 11 shows that the OH density rises steeply at onset of an SEP event. The relative change in the averaged density reaches ~40 to 100% compared with preevent values. For the November 2004 event, OH column density did not decrease to preevent values. We suggested that it could be due to energetic electron precipitation from the radiation belts which is a typical feature of the geomagnetic storm recovery phase, which occurred around 11 through 15 November as seen in the recovery of the *SYM-H* index in Figure 1c. Thus, the role of the associated geomagnetic storm is very important in determining the middle atmospheric response—not only does the storm strength determines the latitudinal extent of the atmospheric response but it is also responsible for the slow recovery as low-energy particles precipitate in the atmosphere well after the end of the SEP.

We did not discuss the possible atmospheric effects of heavy ions accelerated in SEP events. Heavy ions can contribute to the overall ionization of the middle atmosphere, and so possible effects might overlap in time with SPE effects. However, the smaller fluxes of heavy ions as compared to energetic proton fluxes are likely to make their impact relatively small.

Acknowledgments

O.V.'s work was supported by NSF SHINE AGS-0962658 grant and NASA grants EPSCoR NNX09AP74A and NNX11AO64G, the subaward PO 13390 through UAH. S.W. acknowledges the support of the NASA Aura Science Team program. Work at the Jet Propulsion Laboratory, California Institute of Technology, was done under contract to the National Aeronautics and Space Administration. Government Sponsorship acknowledged. M.G.M. would like to acknowledge support from the NASA TIMED project office. The authors acknowledge use of the GOES Space Environment Monitor data provided by NOAA and OMNI database supported by NASA GSFC (at http://omniweb.gsfc.nasa.gov/form/omni_min.html and http://satdat.ngdc.noaa.gov/sem/goes/data/new_avg/). MLS data are provided through http://mls.jpl.nasa.gov/. SABER data are available at http://saber.gats-inc.com/.

Michael Balikhin thanks Hisao Takahashi and another reviewer for their assistance in evaluating this paper.

References

Andersson, M. E., P. T. Verronen, S. Wang, C. J. Rodger, M. A. Clilverd, and B. R. Carson (2012), Precipitating radiation belt electrons and enhancements of mesospheric hydroxyl during 2004–2009, *J. Geophys. Res.*, *117*, D09304, doi:10.1029/2011JD017246.

Andersson, M. E., P. T. Verronen, C. J. Rodger, M. A. Clilverd, and S. Wang (2014), Longitudinal hotspots in the mesospheric OH variations due to energetic electron precipitation, *Atmos. Chem. Phys.*, *14*, 1095.

Cane, H. V., D. V. Reames, and T. T. von Rosenvinge (1988), The role of interplanetary shocks in the longitude distribution of solar energetic particles, *J. Geophys. Res.*, *93*, 9555–9567, doi:10.1029/JA093iA09p09555.

Cohen, C. M. S., G. M. Mason, R. A. Mewaldt, and T. T. von Rosenvinge (2013), Solar energetic particle characteristics and their dependence on longitude in solar cycle 24, *AIP Conf. Proc.*, *1539*, 151, doi:10.1063/1.4811010.
Crutzen, P. J., I. S. A. Isaksen, and G. C. Reid (1975), Solar proton events: Stratospheric sources of nitric oxide, *Science*, *189*, 457.
Damiani, A., M. Storini, M. Laurenza, and C. Rafanelli (2008), Solar particle effects on minor components of the polar atmosphere, *Ann. Geophys.*, *26*, 361–370.
Damiani, A., P. Diego, M. Laurenza, M. Storini, and C. Rafanelli (2009), Ozone variability related to several SEP events occurring during solar cycle no. 23, *Adv. Space Res.*, *43*, 28–40.
Damiani, A., M. Storini, C. Rafanelli, and P. Diego (2010), The hydroxyl radical as an indicator of SEP fluxes in the high-latitude terrestrial atmosphere, *Adv. Space Res.*, *46*, 1225–1235.
Damiani, A., et al. (2012), Impact of January 2005 solar proton events on chlorine species, *Atmos. Chem. Phys.*, *12*, 4159–4179.
Froidevaux, L., et al. (2008), Validation of Aura Microwave Limb Sounder stratospheric ozone measurements, *J. Geophys. Res.*, *113*, D15S20, doi:10.1029/2007JD008771.
Jackman, C. H., M. T. DeLand, G. J. Labow, E. L. Fleming, D. K. Weisenstein, M. K. W. Ko, M. Sinnhuber, and J. M. Russell (2005), Neutral atmospheric influences of the solar proton events in October–November 2003, *J. Geophys. Res.*, *110*, A09S27, doi:10.1029/2004JA010888.
Jackman, C. H., M. T. Deland, G. J. Labow, E. L. Fleming, and M. López-Puertas (2006), Satellite measurements of middle atmospheric impacts by solar proton events in solar cycle 23, *Space Sci. Rev.*, *125*, 381–391.
Jackman, C. H., D. R. Marsh, F. M. Vitt, R. R. Garcia, C. E. Randall, E. L. Fleming, and S. M. Frith (2009), Long-term middle atmospheric influence of very large solar proton events, *J. Geophys. Res.*, *114*, D11304, doi:10.1029/2008JD011415.
Jackman, C. H., et al. (2011), Northern Hemisphere atmospheric influence of the solar proton events and ground level enhancement in January 2005, *Atmos. Chem. Phys.*, *11*, 6153–6166, doi:10.5194/acp-11-6153-2011.
Jackman, C. H., C. E. Randall, V. L. Harvey, S. Wang, E. L. Fleming, M. López-Puertas, B. Funke, and P. F. Bernath (2014), Middle atmospheric changes caused by the January and March 2012 solar proton events, *Atmos. Chem. Phys.*, *14*, 1025–1038, doi:10.5194/acp-14-1025-2014.
Kallenrode, M.-B. (2003), Current views on impulsive and gradual solar energetic particle events, *J. Phys. G: Nucl. Part. Phys.*, *29*, 965.
Kyrölä, E., et al. (2006), Nighttime ozone profiles in the stratosphere and mesosphere by the Global Ozone Monitoring by Occultation of Stars on Envisat, *J. Geophys. Res.*, *111*, D24306, doi:10.1029/2006JD007193.
Leske, R. A., R. A. Mewaldt, E. C. Stone, and T. T. von Rosenvinge (2001), Observations of geomagnetic cut-off variations during solar energetic events and implications for the radiation environment at the Space Station, *J. Geophys. Res.*, *106*, 30,011–30,022, doi:10.1029/2000JA000212.
Li, G., and G. P. Zank (2005), Mixed particle acceleration at CME-driven shocks and flares, *Geophys. Res. Lett.*, *32*, L02101, doi:10.1029/2004GL021250.
Livesey, N. J., V. W. Snyder, W. G. Read, and P. A. Wagner (2006), Retrieval algorithms for the EOS Microwave Limb Sounder (MLS), *IEEE Trans. Geosci. Remote Sens.*, *44*(5), 1144–1155.
Livesey, N. J., et al. (2008), Validation of Aura Microwave Limb Sounder O3 and CO observations in the upper troposphere and lower stratosphere, *J. Geophys. Res.*, *113*, D15S02, doi:10.1029/2007JD008805.
Mannucci, A. J., B. T. Tsurutani, M. A. Abdu, W. D. Gonzalez, A. Komjathy, E. Echer, B. A. Iijima, G. Crowley, and D. Anderson (2008), Superposed epoch analysis of the dayside ionospheric response to four intense geomagnetic storms, *J. Geophys. Res.*, *113*, A00A02, doi:10.1029/2007JA012732.
Pickett, H. M., B. J. Drouin, T. Canty, L. J. Kovalenko, R. J. Salawitch, N. J. Livesey, W. G. Read, J. W. Waters, K. W. Jucks, and W. A. Traub (2006a), Validation of Aura MLS HO*x* measurements with remote-sensing balloon instruments, *Geophys. Res. Lett.*, *33*, L01808, doi:10.1029/2005GL024048.
Pickett, H. M., W. G. Read, K. K. Lee, and Y. L. Yung (2006b), Observations of night OH in the mesosphere, *Geophys. Res. Lett.*, *33*, L19808, doi:10.1029/2006GL026910.
Randall, C. E., D. E. Siskind, and R. M. Bevilacqua (2001), Stratospheric NOx enhancements in the southern hemisphere vortex in winter/spring of 2000, *Geophys. Res. Lett.*, *28*, 2385–2388, doi:10.1029/2000GL012746.
Rong, P. P., J. M. Russell III, M. G. Mlynczak, E. E. Remsberg, B. T. Marshall, L. L. Gordley, and M. Lopez-Puertas (2009), Validation of Thermosphere Ionosphere Mesosphere Energetics and Dynamics/Sounding of the Atmosphere using Broadband Emission Radiometry (TIMED/SABER) v1.07 ozone at 9.6 mm in altitude range 15–70 km, *J. Geophys. Res.*, *114*, D04306, doi:10.1029/2008JD010073.
Rusch, D. W., J.-C. Gérard, S. Solomon, P. J. Crutzen, and G. C. Reid (1981), The effect of particle precipitation events on the neutral and ion chemistry of the middle atmosphere: I. Odd nitrogen, *Planet. Space Sci.*, *29*(7), 767.
Smart, D. F., and M. A. Shea (2005), A review of geomagnetic cutoff rigidities for earth-orbiting spacecraft, *Adv. Space Res.*, *36*, 2012–2020.
Solomon, S., D. W. Rusch, J.-C. Gérard, G. C. Reid, and P. J. Crutzen (1981), The effect of particle precipitation events on the neutral and ion chemistry of the middle atmosphere: II. Odd hydrogen, *Planet. Space Sci.*, *29*(8), 885–893.
Solomon, S., D. W. Rusch, R. J. Thomas, and R. S. Eckman (1983), Comparison of mesospheric ozone abundance measured by the Solar Mesosphere Explorer and model calculations, *Geophys. Res. Lett.*, *10*, 249–252, doi:10.1029/GL010i004p00249.
Sreeja, V., S. Ravindran, T. K. Pant, C. V. Devasia, and L. J. Paxton (2009), Equatorial and low-latitude ionosphere-thermosphere system response to the space weather event of August 2005, *J. Geophys. Res.*, *114*, A12307, doi:10.1029/2009JA014491.
Sugiura, M., and S. Hendricks (1967), Provisional hourly values of equatorial Dst for 1961, 1962m and 1963, *NASA Tech. Note D-4047*.
Turunen, E., P. T. Verronen, A. Seppälä, C. J. Rodger, M. A. Clilverd, J. Tamminen, C.-F. Enell, and T. Ulich (2009), Impact of different energies of precipitating particles on NOx generation in the middle and upper atmosphere during geomagnetic storms, *J. Atmos. Sol. Terr. Phys.*, *71*, 1176–1189.
Tylka, A. J., C. M. S. Cohen, W. F. Dietrich, M. A. Lee, C. G. Maclennan, R. A. Mewaldt, C. K. Ng, and D. V. Reames (2005), Shock geometry, seed populations, and the origin of variable elemental composition at high energies in large gradual solar particle events, *Astrophys. J.*, *625*, 474.
Verkhoglyadova, O. P., and S. Wang (2014), Middle atmosphere response to large SEP events: September 2005 event, in *Outstanding Problems in Heliophysics: From Coronal Heating to the Edge of the Heliosphere, Proceedings of a 12th Annual International Astrophysics Conference, Myrtle Beach, South Carolina, USA*, edited by Q. Hu and G. P. Zank, Astronomical Society of the Pacific Conf. Series, *484*, 207–212, San Francisco, Calif., 14–19 April 2013.
Verkhoglyadova, O. P., G. Li, G. P. Zank, Q. Hu, C. M. S. Cohen, R. A. Mewaldt, G. M. Mason, D. K. Haggerty, T. T. von Rosenvinge, and M. D. Looper (2010), Understanding large SEP events with the PATH code: Modeling of the 13 December 2006 SEP event, *J. Geophys. Res.*, *115*, A12103, doi:10.1029/2010JA015615.
Verkhoglyadova, O. P., G. Li, G. P. Zank, and X. Ao (2013), Modeling of radial dependence of Fe/O elemental abundance ratio in mixed SEP events with the PATH code, *AIP Conf. Proc.*, *1539*, 295, doi:10.1063/1.4811046.
Verronen, P. T., A. Seppala, E. Kyrola, J. Tamminen, H. M. Pickett, and E. Turunen (2006), Production of odd hydrogen in the mesosphere during the January 2005 solar proton event, *Geophys. Res. Lett.*, *33*, L24811, doi:10.1029/2006GL028115.
Verronen, P. T., C. J. Rodger, M. A. Clilverd, H. M. Pickett, and E. Turunen (2007), Latitudinal extent of the January 2005 solar proton event in the Northern Hemisphere from satellite observations of hydroxyl, *Ann. Geophys.*, *25*, 2203–2215.

Verronen, P. T., C. J. Rodger, M. A. Clilverd, and S. Wang (2011), First evidence of mesospheric hydroxyl response to electron precipitation from the radiation belts, *J. Geophys. Res.*, *116*, D07307, doi:10.1029/2010JD014965.

Verronen, P. T., M. E. Andersson, C. J. Rodger, M. A. Clilverd, S. Wang, and E. Turunen (2013), Comparison of modeled and observed effects of radiation belt electron precipitation on mesospheric hydroxyl and ozone, *J. Geophys. Res. Atmos.*, *118*, 11,419–11,428, doi:10.1002/jgrd.50845.

Wang, S., et al. (2013), Atmospheric OH response to the most recent 11-year solar cycle, *Proc. Natl. Acad. Sci. U.S.A.*, *110*, 2023–2028, doi:10.1073/pnas.1117790110.

Waters, J. W., et al. (2006), The Earth Observing System Microwave Limb Sounder (EOS MLS) on the Aura satellite, *IEEE Trans. Geosci. Remote Sens.*, *44*, 1075–1092.

Zank, G. P., G. Li, V. Florinski, Q. Hu, D. Lario, and C. W. Smith (2006), Particle acceleration at perpendicular shock waves: Model and observations, *J. Geophys. Res.*, *111*, A06108, doi:10.1029/2005JA011524.

Zank, G. P., G. Li, and O. P. Verkhoglyadova (2007), Particle acceleration at interplanetary shocks, *Space Sci. Rev.*, *130*, 255–272, doi:10.1007/s11214-007-9214-2.

Zong, Q.-G., X.-Z. Zhou, Y. F. Wang, X. Li, P. Song, D. N. Baker, T. A. Fritz, P. W. Daly, M. Dunlop, and A. Pedersen (2009), Energetic electron response to ULF waves induced by interplanetary shocks in the outer radiation belt, *J. Geophys. Res.*, *114*, A10204, doi:10.1029/2009JA014393.

Zuo, P. B., F. S. Wei, X. S. Feng, X. J. Xu, and W. B. Song (2010), Magnetic cloud boundary layer of 9 November 2004 and its associated space weather effects, *J. Geophys. Res.*, *115*, A10102, doi:10.1029/2009JA014815.